DOI: 10.38027/N11ICCAUA20250143

Chapter 11

Signal Denoising under Environmental Stressors in Heritage Monitoring

* Salvatore Polverino, Hourakhsh Ahmad Nia, Rokhsaneh Rahbarianyazd

Introduction

In modern communication systems, Software Defined Radios (SDRs) are crucial due to their flexibility and adaptability (Aboltins & Tihomorskis, 2023), despite of their vulnerability to low-frequency noise, which can degrade performance, especially in environments with high electromagnetic interference, sustained by Katz and Flynn (2009) who stress the importance of demonstrating communication concepts through SDR, as evidenced by White, Joseph F. (2003), by the use of a structured approach-model which emulates the simulation of circuit behaviour in microwave engineering, as also prompted by Rojhani et al. (2022) and Hu, C. et al. (2016), who offer respectively a detailed examination of location with velocity estimation, and how Kalman-based (Kalman, E., 1960, Chui, C. et al., 1991) channel tracking improves the bit-error-rate (BER) performance using Multiple Input Multiple Output (MIMO) radars in cluttered environments; in this regard, this paper introduces an enhanced SDR architecture, initiated on the premise of block diagrams (Kravchenko, V. et al., 2017), comparing conventional transceivers and a subsampling approach.

To support the hypothesis of mitigating noise, we additionally propose an integrated Kalman filter enhanced adaptively into real-time (Chen, G. et al., 1991) SDR systems, with regard of time-varying autoregressive (AR) coefficients of the signal, which are then used to compute the PSD (Zhang, G. et al., 2006), thoroughly explored by Ermolova (2009), displacing these features in Extended Fisher Information Matrices (FIMs) for real-time adjustments to noise covariance, as discussed by He, J. et al. (2024) Saho K. et al. (2015), Bashirov, E. et al. (2020), a random variable collection typical in stochastic random variables systems (Volosyuk, K. et al., 2018, Chirikjian, Gregory S. 2012); this recent demand, with reference to fine-tuned adaptation, has been critical for maintaining the Kalman filter's robustness (Xiong, et al. (2021), and ensuring accurate state estimation under challenging conditions, as supported by Batra et al. (2004), who analyze the resilience of ultra-wideband (UWB) systems in context-responsive environments (Di Mauro, L. et al., 2024).

Significantly, the proposed block diagram in Figure 1, significant of various schemes such as Relay-and-Antenna Selection (LRAS) by Hu and Kao (2016), improves SDR performance in signal detection and subsampling classification across two environments: the Extended Fisher Information (EFIM), located on the receiver side immediately after the RX (Receive Antenna), values the digital demodulated processing, decoding and advanced algorithms, amplified by Low-Noise Amplifier (LNA), coming from the Digital Signal Processing (DSP) and in first place, the Analog-to-Digital Converter (ADC) (Unbehauen, R. et al., 1989).

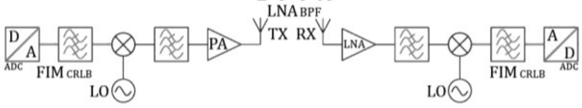

Figure 1. Block Diagram of SDR system incorporating FIM, CRLB, and EFIM.

Corresponding Author: * Salvatore Polverino
Corresponding Author's Department of Department of Architecture, Faculty of Engineering and Natural Sciences, Alanya University, Cikcilli District, Saraybeleni Street No:7 07400, Alanya/Antalya/TÜRKİYE
Corresponding Author's * e-mail: polverinosalvatore@outlook.com

How to Cite This Chapter:
Polverino, S., Ahmad Nia, H., & Rahbarianyazd, R. (2025). Signal denoising under environmental stressors in heritage monitoring. In Rokhsaneh Rahbarianyazd & Hourakhsh Ahmad Nia (Eds.), *Resilient Heritage & Adaptive Urbanism* (pp. 124–135). Cinius Yayınları. https://doi.org/10.38027/N11ICCAUA20250143

This role is to perform the estimation of parameters alongside the FIM, as an integrated part; related to FIM, we configured the Cramér-Rao Lower Bound (CRLB), that performs resourcefully as yielded by Jones, A. et al. (1996) into the theoretical limit on the variance of unbiased $\hat{\theta}$ estimators of EFIM expected value of θ, in E $[\hat{\theta}]$ applied to spin-spin relaxation times, T_1 and T_2.

Methods

To assess the sensitivity of SDR components to low-frequency noise, the Extended Fisher Information Matrices (EFIMs) were employed. The Kalman filter was adapted to dynamically adjust the process and measurement noise covariance matrices in real-time, guided by the EFIMs, forwarding to the cohesive state estimation process, also supported by Xiong, K. et al. (2018). Simulations were conducted across various "deliberate", (Bashirov A., 2003), noise scenarios factoring the analytical Python modules commonly used within the scope of modelling data, such as NumPy, in the process of large arrays and matrices, Matplotlib, as a powerful data visualization tool, Simply, with regard of process-based discrete-event simulation, and TensorFlow, in terms of large-scale simulation data and the extraction of patterns.

Signals were modeled as a linear combination of known waveforms and noise, impacting the localization of front-end positionings, as for wireless sensor networks (WSNs) (Zhang, et al., 2013), in terms of scalability (Gupta, P. et al., 2000), and actualized in parallel to So (2018) whose algorithms are discerned between time-of-arrival (TOA) or time-difference-of-arrival (TDOA). By utilizing the EFIM within a dual Kalman filtering framework, we modelled how different noise environments affect the estimation process in SDRs, translated into electromagnetic interferences by Tse and Viswanath (2005). Specifically, two scenarios were considered: scenario a (Segesta site) and scenario B (Selinunte park). In the optical image of scenario A, multiple interfaces and varying material properties lead to significant signal loss and dispersion, resulting in a lower EFIM and reduced accuracy in estimating signal parameters. In scenario B, the fewer interfaces and lower loss result in a higher EFIM, thereby improving the accuracy of signal estimation and detection capabilities. The mathematical Equation 1 of the observed signal $y\ (t)$ is expressed as:

$$y(t) = \sum_{i=1}^{N} \Gamma_i \cdot T_i \cdot h_i\ (\theta) + n(t)$$ **Equation 1.** Multi-Path Signal Model.

where $h\ (\theta)$ is the signal parameterized by θ (which could represent frequency, amplitude, phase) and $n\ (t)$ is the noise, which varies depending on the scenario. For scenario A and B: $n_{A,B}(t) \sim N(0, \sigma_{A,B}^2)$.
Γ_i is the reflection coefficient at the i-th interface, T_i is the transmission coefficient at the i-th interface and $h_i\ (\theta)$ represents the signal component corresponding to the path through.

1.a. Fisher Information Matrix Extension

The dual Unscented Kalman Filter (UKF) (Wan, A. et al., 2000, Van Der Merwe, R. et al., 2001, Bonnabel, S., 2007).) used can be adapted to account for these Fresnel coefficients, which are critical in predicting signal behavior, by the use of Unscented Transformation (UT), after reflections or transmissions, more conveniently than the Extended Kalman Filter (Julier, S. et al., 1997). The Fisher Information Matrix (FIM) quantifies the information that observable data carries about a parameter, θ. This formulation considers the contributions from different media, each path affecting the overall signal received. For scenarios with varying noise levels, such as urban (high noise) and rural (low noise) environments, the FIM can be adapted. In high noise, FIM values decrease, indicating reduced parameter estimation accuracy. Conversely, in low noise environments, the FIM is higher, improving signal detection.

To address these variations, the FIM is integrated into SDR performance metrics, such as probability of error (PER) and bit error rate (BER). The incorporation of chaotic systems and the use of an extended FIM within a dual Kalman filtering framework allows for dynamic adjustment of noise covariance matrices, improving SDR robustness against low-frequency noise and multipath interference. The key Equation 2, summarises the aforementioned statements:

$$\mathbf{I}(\theta) = \frac{1}{\sigma^2} \sum_{i=1}^{N} \left[\left(\frac{\partial(\Gamma_i \cdot T_i \cdot h_i\ (\theta))}{\partial \theta} \right) \left(\frac{\partial(\Gamma_i \cdot T_i \cdot h_i\ (\theta))}{\partial \theta} \right)^T \right]$$ **Equation 2.** Noise-Adapted Signal Path Estimation Formula.

1.a.I. Optimizing SDR Signal Detection Through FIM-Based Adaptive Algorithms

The FIM-based adaptive algorithms is discussed by Blech et al. (2010) not only quantifying the information content for parameter estimation but also redesigning software-defined ultra-wideband (UWB) transceiver in overcoming the limitations of traditional narrowband systems (Pavlikov, V. et al., 2018) in noisy environments, a common strategy for passive radar systems (Kutuzov, M. et al., 1987) and Magnetic Resonance Imaging (MRI) (Bouhrara, M.

et al., 2018); this aligns with Convex optimization techniques (Boyd, S., & Vandenberghe, L., 2004) and Sadiku and Akujuobi's (2004) observations on the need for a concise overview to instruct azimuth parameters, e.g. location movement or surface characteristics (Pavlikov, V. et al., 2018), and calibrate the adaptive capabilities of SDRs (Ramos-Perez, I. et al., 2012) in Electronic Warfare (EW) contexts, that align to AirComp systems through data fusion (Nazer, B., et al., 2007) and optimal Tx-Rx policy design under power constraints, as issued by Liu et al. (2020).

Serving as a basis for deriving performance bounds, we accounted the Cramér-Rao Lower Bound (CRLB), that provides a lower bound on the variance of unbiased ground estimators, by adopting a parameter adjustment approach inspired by Saho and Masugi (2015); their method utilizes a steady-state performance index that correlates with the root-mean-square prediction error, allowing for more precise tuning of the process noise covariance matrix in the filter.

In support of this empirical dynamic target tracking theorization, Bromiley, P. (2003) discussed in detail the convolution of Gaussian probability density functions to model the impact of noise on signal detection in non-linear (Jinan, R. et al., 2016) systems: in this regard, the FIM for scenarios, A and B, is estimated as the inversely proportional to the noise variance, σ^2, as expressed by Equation 3:

$$\mathbf{I}(\theta) = \frac{1}{\sigma^2}\sum_{i=1}^{N}\left[\left(\frac{\partial S_{21}(\omega,\theta)}{\partial\theta}\right)\left(\frac{\partial S_{21}(\omega,\theta)}{\partial\theta}\right)^T\right]$$ **Equation 3.** Fisher Information Model in Modified Transfer.

The extension of our filtering approach to include differential equations, similar to the PDE-based (Partial Differential Equations) methods used by Bashirov et al. (2008), underscores the importance of advanced mathematical modeling in addressing the intricacies of modern dynamic systems.

Given that $\sigma_A^2 > \sigma_B^2$, we can expect in Scenario A, with higher noise results in a lower FIM, leading to a higher Probability of Error (PER) and Bit Error Rate (BER), while scenario B benefits from a higher FIM, indicating better signal detection accuracy.

Moreover, the integration of chaotic systems into SDRs, modeled by the chaotic spread spectrum technique coupled with the Kalman filter, further enhances signal processing robustness against low-frequency noise and multipath interference. The refined model can be extended to Ultra-Wideband (UWB) scenarios, incorporating transfer functions for the transmitter and receiver antennas, also confirmed, respectively, in Equation 4:

$$H_{N,\mathrm{new,TX}}(\omega) = \frac{j\,\omega}{c_0}\sqrt{\frac{\omega}{\pi}}\,H_{N,\mathrm{new,TX}}(\omega);$$ **Equation 4.** Transfer Function of the Transmitter Antenna.

Whilst the transfer function of the communication channel is represented in Equation 5, for how the signal is altered as it travels through the channel, taking into account $T_i(\omega)$, the transmission coefficient, $\Gamma_i(\omega)$, the frequency-dependent reflection coefficient at the *i*-th interface and τ_i represents the delay associated with the *i*-th path.

$$H_{CH}(\omega) = \sum_{i=1}^{N}\Gamma_i(\omega)\cdot T_i(\omega)\cdot e^{-j\omega\tau_i};$$ **Equation 5.** Transfer Function.

The overall transmission parameter, $S_{21}(\omega)$ stressed mathematically in Equation 6, characterizes the communication link, with the effects of Fresnel coefficients and environmental variations:

$$h(\theta) \to S_{21}(\omega) = H_{N,new,TX}\cdot(\omega)\,H_{CH}(\omega)\cdot H_{N,new,RX}(\omega);$$ **Equation 6.** Communication link S_{21}.

1.a.II. Extended model in UWB systems

The FIM for this comprehensive model is given by a refinement of overall frequency-dependent effects as reported in Equation 7: reflections, transmissions, and path delays, allow for precise parameter estimation even in complex environments. In parallel, the CRLB, derived from the FIM, provides insights into the achievable precision of parameter estimation, guiding the design of more resilient SDR systems.

$$(\theta) = \frac{1}{\sigma^2}\sum_{i=1}^{N}\left(\frac{\partial\left(\frac{j\omega}{c_0}\sqrt{\frac{\omega}{\pi}}\,H_{N,new,TX}(\omega)\cdot\sum_{i=1}^{N}\Gamma_i(\omega)\cdot T_i(\omega)\cdot e^{-j\omega\tau_i}\cdot\frac{1}{c_0}\sqrt{\frac{\omega}{\pi}}H_{N,new,RX}(\omega)\right)}{\partial\theta}\right)$$

Equation 7. Derivative version of the Fisher Information Model parameterization in UWB.

1.a.III. Adaptive Noise Mitigation in SDRs with Extended Fisher Information Matrix

By deriving the Cramér-Rao Lower Bound (CRLB) from the FIM, determining the minimum variance achievable for unbiased estimators, $\mathrm{Var}\left(\hat{\theta}\right) \geq \mathrm{CRLB} = \frac{1}{I(\theta)}$. The observed signal y is modeled as $y = h\,(\theta) + n$. The Fisher Information Matrix (FIM) is given by Equation 8:

$$\mathbf{I}(\theta) = \frac{1}{\sigma^2}\left(\frac{\partial h\,(\theta)}{\partial \theta}\right)^2$$ **Equation 8.** FIM-Based Analysis of Signal Parameter Sensitivity.

Using basic parameters $h\,(\theta) = \theta^{\,2}$ and $\sigma^{\,2} = 1$, the FIM is $4\,\theta^{\,2}$, and the CRLB is $1/4\,\theta^{\,2}$. By refining the model and increasing the Signal-to-Noise Ratio (SNR), the CRLB is reduced further, showing improved estimation precision. With data fusion techniques doubling the FIM, the CRLB can be minimized, leading to even greater accuracy in signal estimation.

1.a.IV. FIM and Kalman Filtering for Enhanced State Estimation in SDRs

The Fisher Information Matrix (FIM) is tightly linked to the Cramér-Rao Lower Bound (CRLB), offering a lower bound on the variance of unbiased estimators, as for indicating how the estimation of one parameter influences the estimation of another, i.e. $\mathrm{I}_{\theta_m\theta_m} = {}^{1}\!/_{\mathrm{CRLB}(\theta_m)}$ along the off-diagonal .

By incorporating parameters, θ_{m}, ϵ_{rm}, ϕ, d_{pvm}, d_{GHm}, the FIM captures the covariance between these parameters, reflecting their interactions under a Rayleigh clutter model or similar scenarios joint estimation. The Kalman filter, integrated with the FIM, improves state estimation by dynamically adjusting the process and measurement noise covariance matrices. This is essential in low-frequency noise environments, where the Kalman filter updates state predictions and corrections to maintain accuracy.

The association of such prediction-correction model, where it predicts the state based on a previous state and corrects it using current measurements, is integrated in terms of covariance between the parameters and their dynamic state estimations by adding Kalman gain, K_{θ_m}, for the parameter θ_m, reflecting how the Kalman filter adjusts the state estimate based on new observations; its updated form is presented in Equation 9 while the measurement update follows in Equation 10:

$$\mathrm{P}_{k|k-1} = F_k\, P_{\,k-1|k-1}\, F_k^T + Q_k(I_{LF})$$ **Equation 9.** Covariance Matrix Update for State Prediction.

$$K_k = P_{k|k-1}\, H^T (H P_{k|k-1}\, H^T + R)^{-1}$$ **Equation 10.** State Correction Gain in Kalman Filtering.

By incorporating in FIM, stated in Equation 11, we observe $\mathrm{P}_{k|k-1}$, that represents the predicted error covariance matrix, K_k, the Kalman gain, and H_k , the observation matrix.

$$FIM_{Kalman} = \begin{pmatrix} \frac{1}{CRLB(\theta_m)} + K_{\theta_m} & Cov(\theta_m, \epsilon_{rm}) + K_{\theta_m,\epsilon_{rm}} & Cov(\theta_m, \phi) + K_{\theta_m,\phi} & Cov(\theta_m, d_{pvm}) + K_{\theta_m,d_{pvm}} & Cov(\theta_m, d_{GHm}) + K_{\theta_m,d_{GHm}} \\ Cov(\epsilon_{rm}, \theta_m) + K_{\epsilon_{rm},\theta_m} & \frac{1}{CRLB(\epsilon_{rm})} + K_{\epsilon_{rm}} & Cov(\epsilon_{rm}, \phi) + K_{\epsilon_{rm},\phi} & Cov(\epsilon_{rm}, d_{pvm}) + K_{\epsilon_{rm},d_{pvm}} & Cov(\epsilon_{rm}, d_{GHm}) + K_{\epsilon_{rm},d_{GHm}} \\ Cov(\phi, \theta_m) + K_{\phi,\theta_m} & Cov(\phi, \epsilon_{rm}) + K_{\phi,\epsilon_{rm}} & \frac{1}{CRLB(\phi)} + K_{\phi} & Cov(\phi, d_{pvm}) + K_{\phi,d_{pvm}} & Cov(\phi, d_{GHm}) + K_{\phi,d_{GHm}} \\ Cov(d_{pvm}, \theta_m) + K_{d_{pvm},\theta_m} & Cov(d_{pvm}, \epsilon_{rm}) + K_{d_{pvm},\epsilon_{rm}} & Cov(d_{pvm}, \phi) + K_{d_{pvm},\phi} & \frac{1}{CRLB(d_{pvm})} + K_{d_{pvm}} & Cov(d_{pvm}, d_{GHm}) + K_{d_{pvm},d_{GHm}} \\ Cov(d_{GHm}, \theta_m) + K_{d_{GHm},\theta_m} & Cov(d_{GHm}, \epsilon_{rm}) + K_{d_{GHm},\epsilon_{rm}} & Cov(d_{GHm}, \phi) + K_{d_{GHm},\phi} & Cov(d_{GHm}, d_{pvm}) + K_{d_{GHm},d_{pvm}} & \frac{1}{CRLB(d_{GHm})} + K_{d_{GHm}} \end{pmatrix}$$

Equation 11. Fisher Information Model comprehensive of Kalman and CRLB.

1.b.I. FIM-Based Signal Estimation in UWB Systems with Complex Path Interactions

These modifications enable the Kalman filter to maintain high accuracy in state estimation despite the presence of low-frequency noise, proposing a novel FIM expression, otherwise detailed inside the partial derivative $\frac{\partial}{\partial\theta}$ in the context of Ultra-Wideband (UWB) with respect to the parameter θ, by summating multiple reflections, transmissions, or paths indexed by *I*, in a multipath environment, by incorporating in Equation 12: i) $\frac{1}{\sigma^2}$, our normalized Inverse Noise Variance, which scales the FIM by the noise variance σ^2; ii) angular frequency ω, the speed of light c_0, and a frequency-dependent scaling factor $\frac{j\omega}{c_0}$ – both of them are related to a unique term which introduces a phase component to the UWB signal propagation; iii) $H_{N,new,TX}(\omega)$, or Transmitter Transfer Function, normalizing as a transfer function of the transmitting antenna, in the same manner, representing how the signal is affected by the transmitting hardware; iv) $\sum_{i=1}^{N} \Gamma_i(\omega) \cdot T_i(\omega) \cdot$

$e^{-j\omega\tau_i}$, or Summed Reflections and Transmissions, composed by $\Gamma_i(\omega)$ – the reflection coefficient at the i-th interface, representing the portion of the signal that is reflected – $T_i(\omega)$, the transmission coefficient, and $e^{-j\omega\tau_i}$, the phase shift due to the time delay τ_i, accounting the signal's travel time and phase change over the distance; v) $\frac{1}{c_0}\sqrt{\frac{\omega}{\pi}}H_{N,new,RX}(\omega)$, a term inclined to the front-end connotation, representing how the signal is affected by the receiving hardware.

$$\mathbf{I}(\theta) = \frac{1}{\sigma^2}\sum_{i=1}^{N}\left(\frac{\partial}{\partial\theta}\left[\left(\frac{j\omega}{c_0}\sqrt{\frac{\omega}{\pi}}\,H_{N,new,TX}(\omega)\cdot\sum_{i=1}^{N}\Gamma_i(\omega)\cdot T_i(\omega)\cdot e^{-j\omega\tau_i}\cdot\frac{1}{c_0}\sqrt{\frac{\omega}{\pi}}H_{N,new,RX}(\omega)\right)\right]\right)^2$$

Equation 12. Frequency-Dependent FIM in UWB Systems with Path-Based Distortions.

1.b.II. Covariances for FIM indicates parameters and CRLB (Cramer-Rao Lower Bound)

The measurement variances integrated the theoretical model (Pogorelyuk, L. et al., 2021) through a Kalman filter approach: i) the process started from relevant features from the Figures 2 and 3, establishing for orientation θ_m, computed as 90 degrees, bounding box area, 68,055 square pixels to infer size-related parameters like distance and edge detection which is estimated in terms of variance, e.g. $Cov(\theta_m, \phi)$;

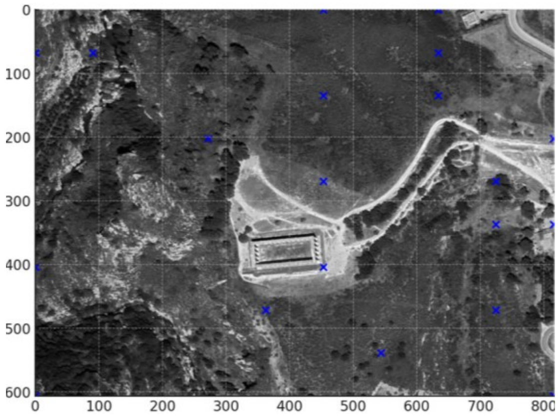

Figure 2. FIM_1 orientation.

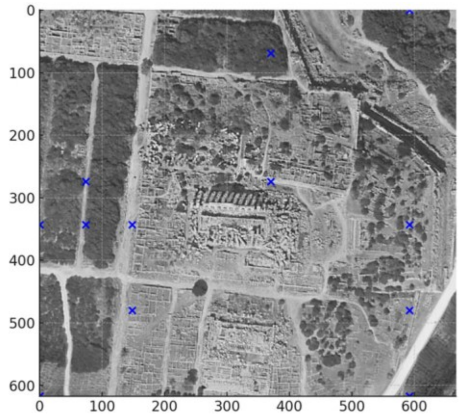

Figure 3. FIM_2 orientation.

ii) in the second instance, the FIM matrix incorporated the variability in the detected edges, orientation across multiple observations, as from the Kalman filter and CRLB for bounding box's precision; iii) critical of this theoretical approach, was the time-series requirement data, for which a simplified approach considered: a) the variance in orientation, θ_m, in parallel to precision in the Bounding image processing; b) covariances based on potential correlations between orientation and edge detection; c) Kalman filter' application refined in a Bayesian robust estimation (Durovic, M. et al., 1999); iv) the incorporation of CRLB parameters deliver the two corresponding FIMs, given in Equation 13 and 14, with parameters listed in Table 1.

$$\mathrm{FIM}_{\mathrm{Segesta}} = \begin{pmatrix} 3.00 & 1.10 & 1.05 & 1.02 & 1.03 \\ 1.10 & 4.33 & 1.08 & 1.04 & 1.03 \\ 1.05 & 1.08 & 3.50 & 1.04 & 1.07 \\ 1.02 & 1.04 & 1.04 & 6.00 & 1.03 \\ 1.03 & 1.03 & 1.07 & 1.03 & 2.67 \end{pmatrix}$$

Equation 13. FIM_1 Covariance values.

$$\mathrm{FIM}_{\mathrm{Selinunte}} = \begin{pmatrix} 2.43 & 1.15 & 1.10 & 1.03 & 1.05 \\ 1.15 & 3.50 & 1.12 & 1.06 & 1.05 \\ 1.10 & 1.12 & 3.00 & 1.06 & 1.10 \\ 1.03 & 1.06 & 1.06 & 4.33 & 1.05 \\ 1.05 & 1.05 & 1.10 & 1.05 & 2.25 \end{pmatrix}$$

Equation 14. FIM_2 Covariance values.

Table 1. CRLBs parameters.

	θ_m	ϵ_{rm}	ϕ	d_{pvm}	d_{GHm}
FIM_1	0.5	0.3	0.4	0.2	0.6
FIM_2	0.7	0.4	0.5	0.3	0.8

Visually, Figures 4 and 5 respectively report the densities registering a higher density of Selinunte, with one of the clusters characterized by a very tightly packed points, which could be due to specific image features or noise.

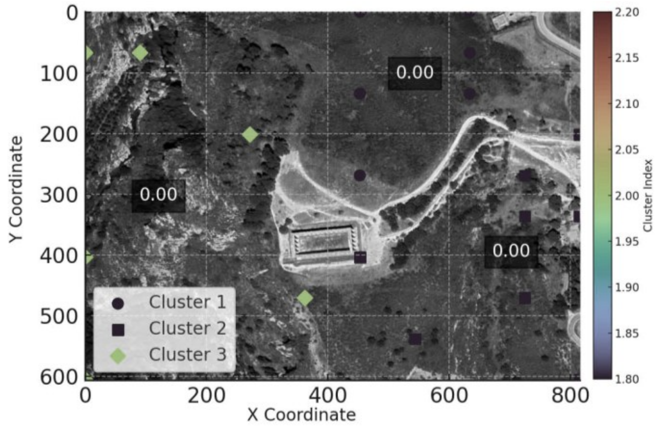

Figure 4. FIM1 Covariance mapping.

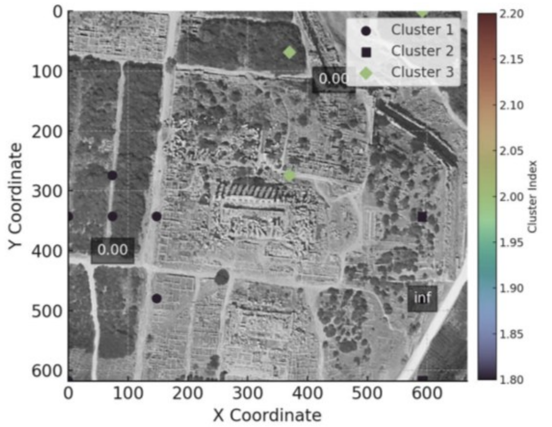

Figure 5. FIM2 Covariance mapping.

In parallel to this, the aggregated covariance matrices for each cluster are quantified as follows in Table 2 with a mismatch for Cluster 2, 0.0000905 and infinity, respectively due to image limitations.

Table 2. Densities.

$\begin{bmatrix} 0.5 & 0.231 \\ 133.2 & 0.12 \end{bmatrix}$	1 FIM 1)	0.000164	$\begin{bmatrix} 0.5 & 0.228 \\ 134.7 & 0.12 \end{bmatrix}$	1 FIM 2)	000169
$\begin{bmatrix} 0.5 & 0.240 \\ 135.6 & 0.12 \end{bmatrix}$	2 FIM 1)	0.0000905	$\begin{bmatrix} 0.5 & 0.240 \\ 129.7 & 0.12 \end{bmatrix}$	2 FIM 2)	infinity
$\begin{bmatrix} 0.5 & 0.253 \\ 133.2 & 0.12 \end{bmatrix}$	3 FIM 1)	0.0000447	$\begin{bmatrix} 0.5 & 0.231 \\ 136.9 & 0.12 \end{bmatrix}$	3 FIM 2)	0.000131

Regarding the Gaussian Mixture Model (GMM) Silhouette, we registered for the first scenario, portrayed in Figure 6, a score equivalent to 0.32, while 0.38 for the second, represented by Figure 7, yielding positive silhouette scores in both images, indicating that the clusters, (K), identified by GMM are reasonably well-separated and well-defined and capturing the structure of the data in both scenarios by sampling two critical parameters (Smiti, A. et al., 2012): ϵ (Eps), the neighbourhood radius, and *MinPts*, the minimum number of points required to form a cluster.

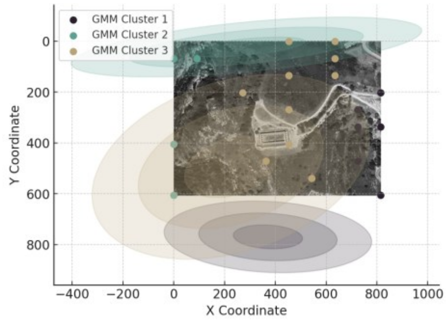

Figure 6. FIM1: GMM DBSCAN.

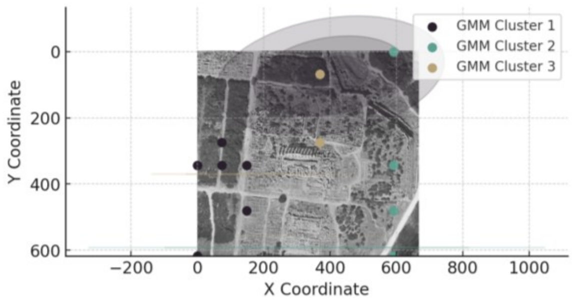

Figure 7. FIM2: GMM DBSCAN.

This visual enhancement of Density-Based Spatial Clustering of Applications with Noise (DBSCAN), particularly effective in handling noise and identifying clusters of arbitrary shapes as for optical and SAR images, (Hu, H. et al., 2017), was incentivized by the adoption of a Bayesian Kalman Filter which incorporated prior distributions into the estimation process, providing a more informed and potentially more accurate estimate, especially when prior knowledge is relevant, which is represented in Equations 15 and 16, with regard of posterior mean estimate of the state $\hat{x}_{k|k}$ at time k, given the observations z_k, and the second, the posterior covariance matrix $P_{k|k}$, which quantifies the uncertainty associated with the state estimate $\hat{x}_{k|k}$:

$$\hat{x}_{k|k} = \int \theta P(\theta \mid z_k)\, d\theta$$ **Equation 15.** Posterior Mean Estimate in Bayesian Filtering.

$$P_{k|k} = \int (\theta - \hat{x}_{k|k})(\theta - \hat{x}_{k|k})^T P(\theta \mid z_k)\, d\theta$$ **Equation 16.** Covariance Matrix Update in Bayesian Estimation.

1.c. Frequency-Specific Noise Impact on RF Signal Processing

This flexibility of software-defined ultra-wideband (UWB) is a core advantage of software-defined radios (SDRs) in UWB systems within the frequency range spanning from 0 to 3 GHz, which covers the spectrum of interest for high-frequency communication systems, including the third Nyquist zone, here designated in correspondence of the Kalman and theta features given in both scenarios.

The use of a high-pass filter with a cut-off frequency of 2.15 GHz, mentioned in Figure 8, is designed to suppress unwanted spectral components below 2 GHz with considerable heavy-tailed distribution (Hongpo F. et al., 2022).

The Power Spectral Density (PSD) evaluation based on Kalman ground estimators (Aboy, M. et al., 2004) given in Figure 8, is now defined as indicated in the graph of Figure 1, in the filtering of the digital demodulated processing, decoding and advanced algorithms, where valleys below 2 GHz appear in both AOI 1 and AOI 2, reflecting the effectiveness of the filtering process, whose quantization process of mapping to discrete leves, leading to a loss of information is also theorized by Romero, D. et al. (2017).

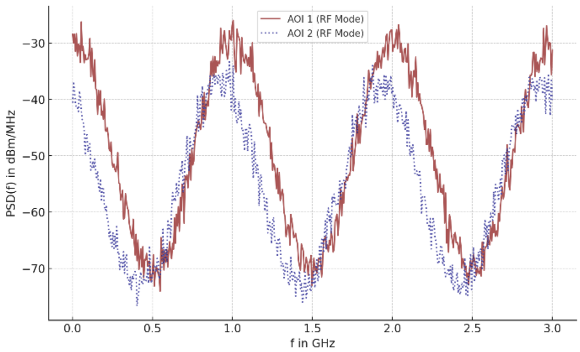

Figure 8. Power Spectral Density of RF Mode in AO1 1 and 2.

The significant attenuation observed below 2 GHz indicates that the filter is performing as expected, reducing the power of signals in that frequency range, which aligns with the behaviour of a high-pass filter. Overall, the statements provided are consistent with the graphical evidence, effectively explaining the function and performance of the UWB transceiver and the associated high-pass filtering process, into how DGS can be used to achieve desired filter characteristics such as sharp roll-off and compact size for performance improvement (Wanchun, T. et al., 2012) (Federal Communication, Commission, 2002).

2. Signal Variability in UWB Networks

Amplified by Low-Noise Amplifier (LNA), retrieved from the Digital Signal Processing (DSP) and the Analog-to-Digital Converter (ADC), the comparison of the UWB network efficiency between first and second Area-of-Interest finds place, revealing distinct differences in both the spatial distribution of signal power and temporal signal stability. In the Segesta dataset, the mean normalized signal power, μ_1, is calculated to be 0.327, indicating a lower average signal strength across the measured area. This lower signal strength is coupled with a standard deviation, σ_1, of 0.170, reflecting a relatively high variability in the signal power.

This variability, expressed in Figure 9 and 10, suggests significant fluctuations in the UWB network performance within the Segesta environment, likely due to non-uniformities in the spatial coverage and potential interference from environmental factors.

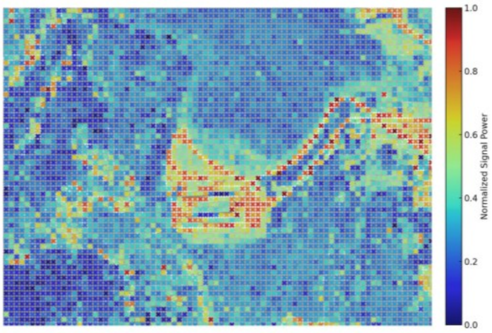

Figure 9. UWB_1' Repeaters.

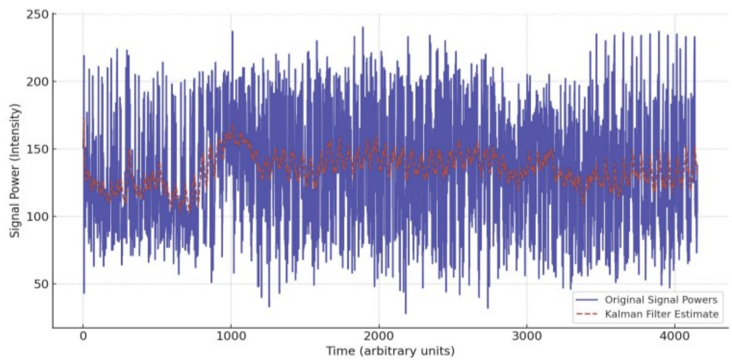

Figure 10. UWB Efficiency.

In contrast, the Selinunte dataset, represented in Figure 11, exhibits a higher mean normalized signal power, highlighted in Figure 12, μ_2, of 0.452, indicating a more robust and consistently stronger UWB network performance. The standard deviation in this scenario, σ_2, is slightly lower at 0.169, compared to Segesta, signifying a marginally more stable signal with less fluctuation in power levels.

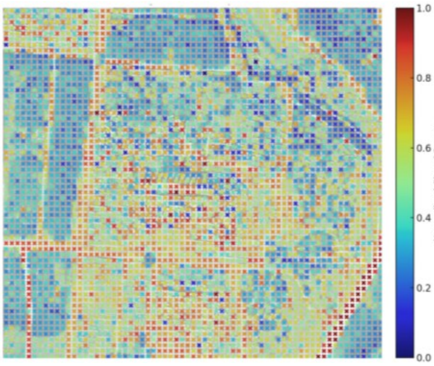

Figure 11. UWB$_2$' Repeaters.

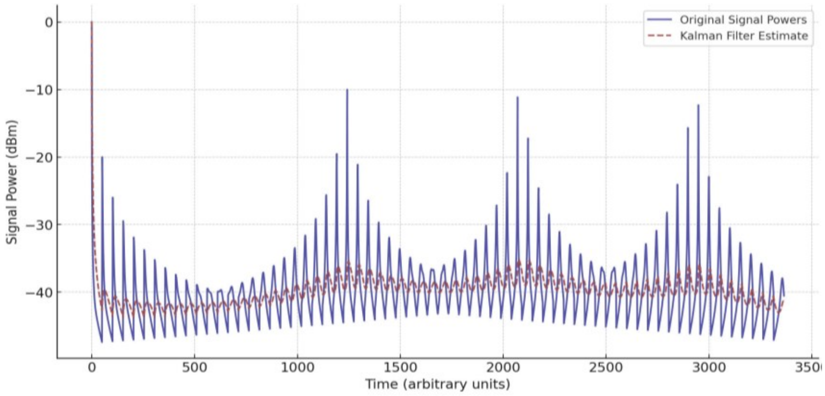

Figure 12. UWB Efficiency.

The difference in mean signal power, $\Delta\mu$ = 0.125, underscores the superior signal quality of the first context, suggesting that the UWB network in this area benefits from better spatial coverage and fewer disruptions. The blended 3D visualization, obtained in Figure 13, enables a direct comparison of signal power distributions across the two scenarios within the same spatial domain: for instance, regions where the Z-axis values are higher indicating stronger signal power, suggesting more effective UWB coverage.

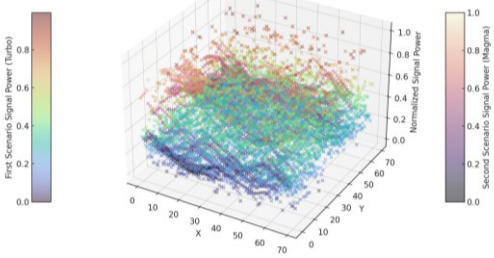

Figure 13. UWB Network Efficiency across the two scenarios.

The overlap of color schemes in certain spatial regions highlights areas of convergence or divergence in signal strength between Segesta and Selinunte.

Frequency-Specific Noise Impact on RF Signal Processing

The Kalman filter needs to account for these discrete components when predicting and correcting the signal, so that starting from the Power Spectral Density (PSD), we initially calculated the comparisons, employing a simpler approach based on the Fourier Transform (FFT), given in Equation 17,

$$X(f) = \sum_{n=0}^{N-1} x(n) \cdot e^{-j\,2\,\pi\,fn/N}$$ **Equation 17.** Fourier Transform.

where $x\,(n)$ is the time-domain signal, N is the number of samples across the two contexts, and $X\,(f)$ is the Fourier Transform of the signal. The corresponding PSD was subsequently computed as the magnitude squared of the FFT in the following Equation 18, related to Figure 14,

$$PSD(f) = |X(f)|^2$$ **Equation 18.** Fourier Transform.

and converted to decibels (dBs) in Equation 19 and 20, related respectively to Figure 15:

$$PSD_{dB}(f) = 10 \cdot\ log_{10}(PSD(f))$$ **Equation 19.** Fourier Transform.

$$\text{PSD}\ (f) = \frac{\sigma_b^2}{T_{sym}} \left|G_{S,RF}(f)\right|^2 \frac{1}{Z_c} + \frac{\mu_b^2}{T_{sym}^2} \sum_{m=-\infty}^{\infty} \left|G_{S,RF}(f)\right|^2 \frac{1}{Z_c} \delta\left(f - \frac{m}{T_{sym}}\right)$$ **Equation 20.** Power Spectral of RF.

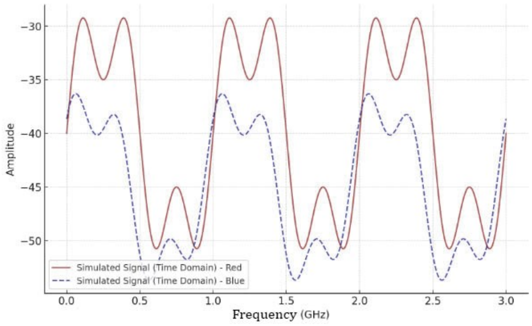

Figure 14. FFT Magnitude of PSD.

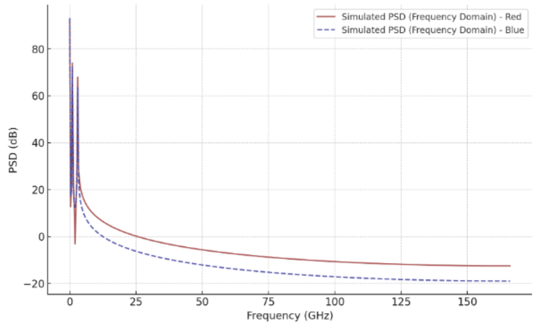

Figure 15. PSD converted to dB.

Conclusion

The integration of extended Fresnel Interface Models (FIMs) into SDR systems effectively mitigates low-frequency noise, enhancing system resilience in challenging environments, particularly urban areas with prevalent multipath effects. The adaptive Kalman filter, augmented with Fresnel coefficients, improves signal detection sensitivity, even for weaker signals affected by multiple reflections. By the same token, comparative analysis shows that the Gaussian Mixture Model (GMM) outperforms DBSCAN in cluster identification, as indicated by positive silhouette scores and clear visual clustering. Accordingly, the proposed approach strengthens SDR systems, escalating against diverse noise conditions, offering a robust solution for RF signal processing.

Acknowledgement

This research did not receive any specific grant from funding agencies in the public, commercial, or not-for-profit sectors. It was initiated through a joint agreement between the Department of Architecture at the Hamdullah Emin Paşa Campus of Alanya University and the Department for Training and Internationalization of the *Ordine degli Architetti, Pianificatori, Paesaggisti e Conservatori* of Naples and its Province, Italy, recognized under Royal Decree No. 2537 of October 23, 1925.

All images included in this work were created by the primary author. Acknowledgements are extended to all peers who contributed to the development of an accessible research methodology, with special thanks to the two anonymous reviewers for their insightful evaluation of the proposed framework.

Conflict of Interests

The authors declare no conflict of interest. The numerical results and their processing do not imply any responsibility in terms of the design, collection, or interpretation of data, but are exclusively intended to demonstrate appropriate and well-calibrated methodologies in support of *Valutazione di Impatto Ambientale* (VIA, Environmental Impact Assessment) and *Valutazione Ambientale Strategica* (VAS, Strategic Environmental Assessment). The research endorses the reintroduction of historically coherent and ecologically compatible components of infrastructures, promoting a sustainable approach to land use, and adopts data extraction methods that exclude animal experimentation and avoid environmentally invasive procedures, in full compliance with the rigorous Italian legislation on landscape protection.

Ethics statements

This study was conducted in accordance with the principles outlined in the European Code of Ethics for Scientific Research and adheres to the Declaration of Helsinki (2013). It received approval from the appropriate Institutional Review Board.

The research posed no harm or risk to participants, and all data collected were used solely to investigate the built environment in relation to Heritage Architecture. All data are strictly unclassified and have been made publicly available without any violation of copyright or intellectual property rights.

For any inquiries or concerns regarding the study, please refer to the official contact details of the hosting university.

References

Aboltins, Arturs, and Nikolajs Tihomorskis. (2023). Software-Defined Radio Implementation and Performance Evaluation of Frequency-Modulated Antipodal Chaos Shift Keying Communication System. *Electronics* 12, fasc. 5: 1240. https://doi.org/10.3390/electronics12051240.

Aboy, M., J. McNames, O.W. Marquez, R. Hornero, T. Thong, and B. Goldstein. (2004). Power spectral density estimation and tracking nonstationary pressure signals based on Kalman filtering. In *The 26th Annual International Conference of the IEEE Engineering in Medicine and Biology Society*, 3:156–59. San Francisco, CA, USA: IEEE. https://doi.org/10.1109/IEMBS.2004.1403115.

Bashirov, Agamirza E. (2003). *Partially Observable Linear Systems Under Dependent Noises*. Basel: Birkhäuser Basel. https://doi.org/10.1007/978-3-0348-8022-0.

Bashirov, Agamirza E., and Kanda Abuassba. (2020). Invariant Kalman Filter for Correlated Wide Band Noises. *Asian Journal of Control* 22, fasc. 2 : 648–56. https://doi.org/10.1002/asjc.1949.

Bashirov, Agamirza, Zeka Mazhar, and Sinem Ertürk. (2008). Boundary Value Problems Arising in Kalman Filtering. *Boundary Value Problems* 2008 : 1–10. https://doi.org/10.1155/2008/279410.

Batra, A., J. Balakrishnan, and A. Dabak. (2004). Multi-band OFDM: a new approach for UWB. In *2004 IEEE International Symposium on Circuits and Systems (IEEE Cat. No.04CH37512)*, V-365-V–368. Vancouver, BC, Canada: IEEE. https://doi.org/10.1109/ISCAS.2004.1329538.

Blech, M. D., A. T. Ott, P. Neumeier, M. Möller, and T. F. Eibert. (2010). A Reconfigurable Software Defined Ultra-Wideband Impulse Radio Transceiver. *Advances in Radio Science* 8: 67–73. https://doi.org/10.5194/ars-8-67-2010.

Bromiley, P. (2003). P. Products and convolutions of Gaussian probability density functions. Tina-Vis. Memo, vol. 3, no. 4, pp. 1–13, 2003.

Bonnabel, Silvere. (2007). Left-invariant extended Kalman filter and attitude estimation. In *2007 46th IEEE Conference on Decision and Control*, 1027–32. New Orleans, LA, USA: IEEE. https://doi.org/10.1109/CDC.2007.4434662.

Boyd, Stephen, and Lieven Vandenberghe. (2004). *Convex Optimization*. 1ª ed. Cambridge University Press. https://doi.org/10.1017/CBO9780511804441.

Bouhrara, Mustapha, and Richard G. Spencer. (2018). Fisher Information and Cramér-Rao Lower Bound for Experimental Design in Parallel Imaging. *Magnetic Resonance in Medicine* 79, fasc. 6 : 3249–55. https://doi.org/10.1002/mrm.26984.

Chen, G., and C.K. Chui. (1991). A modified adaptive Kalman filter for real-time applications. *IEEE Transactions on Aerospace and Electronic Systems* 27, fasc. 1 : 149–54. https://doi.org/10.1109/7.68157.

Chirikjian, Gregory S. (2012). *Stochastic Models, Information Theory, and Lie Groups, Volume 2: Analytic Methods and Modern Applications*. Applied and Numerical Harmonic Analysis. Boston: Birkhäuser Boston. https://doi.org/10.1007/978-0-8176-4944-9.

Chui, Charles K., and Guanrong Chen. (1991). *Kalman Filtering*. Vol. 17. Springer Series in Information Sciences. Berlin, Heidelberg: Springer Berlin Heidelberg. https://doi.org/10.1007/978-3-662-02666-3.

Di Mauro, L., Ahmad Nia, H., Capobianco, L., Polverino, S. and Coppola, A. (2024). Context-responsive decision-making to enhance Multilateral Agreements in Core Principles Cultural Heritage Preservation. In Innovative Approaches to Cultural Heritage and Sustainable Urban Development: Integrating Tradition and Modernity (Integrating Tradition and Modernity, Chapter 21). Cinius Yayınları. https://doi.org/10.38027/N21ICCAUA2024EN0001.

Durovic, Z.M., and B.D. Kovacevic. (1999). Robust estimation with unknown noise statistics. *IEEE Transactions on Automatic Control* 44, fasc. 6 : 1292–96. https://doi.org/10.1109/9.769393.

Ermolova, N. (2009). Spectral analysis of a memory RF power amplifier with Gaussian inputs. In *2009 Wireless Telecommunications Symposium*, 1–4. Prague: IEEE. https://doi.org/10.1109/WTS.2009.5355510.

Federal Communication Commission, Revision of Part 15 of the Commission's Rules Regarding Ultra-Wideband Transmission Systems, Cover Rep. ET-Docket 98-153, FCC 02-48, Apr. 2002.

Fu, Hongpo, and Yongmei Cheng. (2022). A Novel Robust Kalman Filter Based on Switching Gaussian-Heavy-Tailed Distribution. *IEEE Transactions on Circuits and Systems II: Express Briefs* 69, fasc. 6 : 3012–16. https://doi.org/10.1109/TCSII.2022.3161263.

Gupta, P., and P.R. Kumar. (2000). The capacity of wireless networks. *IEEE Transactions on Information Theory* 46, fasc. 2 : 388–404. https://doi.org/10.1109/18.825799.

He, Jiajun, Dominic K. C. Ho, Wenxin Xiong, Hing Cheung So, and Young Jin Chun. (2024). Cramér–Rao Lower Bound Analysis for Elliptic Localization With Random Sensor Placements. *IEEE Transactions on Aerospace and Electronic Systems* 60, fasc. 4 : 5587–95. https://doi.org/10.1109/TAES.2024.3370890.

Hu, Chia-Chang, and Yi-Chi Kao. (2016). Kalman-based relay/antenna selection for two-way MIMO-relay networks. In *2016 IEEE 5th Global Conference on Consumer Electronics*, 1–4. Kyoto, Japan: IEEE. https://doi.org/10.1109/GCCE.2016.7800484.

Hu, Hao, Bin Liu, Weiwei Guo, Zenghui Zhang, and Wenxian Yu. (2017). Superpixel generation for SAR images based on DBSCAN clustering and probabilistic patch-based similarity. In *2017 IEEE International Geoscience and Remote Sensing Symposium (IGARSS)*, 803–6. Fort Worth, TX: IEEE. https://doi.org/10.1109/IGARSS.2017.8127074.

Institute of Electrical and Electronics Engineers, Institute of Electrical and Electronics Engineers, and Adhiparasakthi Engineering College. (2013). a c. di. *2013 International Conference on Communication and Signal Processing (ICCSP 2013): Melmaruvathur, India, 3 - 5 April 2013 ; [Proceedings]*. Piscataway, NJ: IEEE.

Islam, Syed Aseem Ul, Ankit Goel, and Dennis S. Bernstein. (2020). Real-Time Implementation of the Optimal Predictor and Optimal Filter: Accuracy Versus Latency [Lecture Notes]. *IEEE Control Systems* 40, fasc. 2 : 84–91. https://doi.org/10.1109/MCS.2019.2961588.

Jinan, Rooji, and Tara Raveendran. (2016). Particle Filters for Multiple Target Tracking. *Procedia Technology* 24 : 980–87. https://doi.org/10.1016/j.protcy.2016.05.215.

Jones, J.A., P. Hodgkinson, A.L. Barker, and P.J. Hore. (1996). Optimal Sampling Strategies for the Measurement of Spin–Spin Relaxation Times. *Journal of Magnetic Resonance, Series B* 113, fasc. 1 : 25–34. https://doi.org/10.1006/jmrb.1996.0151.

Julier, Simon J., and Jeffrey K. Uhlmann. (1997). New extension of the Kalman filter to nonlinear systems. a cura di Ivan Kadar, 182. Orlando, FL, USA. https://doi.org/10.1117/12.280797.

Kalman, R. E. (1960). A New Approach to Linear Filtering and Prediction Problems. *Journal of Basic Engineering* 82, fasc. 1 : 35–45. https://doi.org/10.1115/1.3662552.

Katz, Sharlene, and James Flynn. (2009). Using software defined radio (SDR) to demonstrate concepts in communications and signal processing courses. In *2009 39th IEEE Frontiers in Education Conference*, 1–6. San Antonio, TX, USA: IEEE. https://doi.org/10.1109/FIE.2009.5350716.

Kravchenko, V. F., B. G. Kutuza, V. K. Volosyuk, V. V. Pavlikov, and Kiem Nguyen Van. (2017). Multiantenna radiometric complex for high resolution imaging: Synthesis of algorithm for optimal UWB signal processing and development of functional flow block diagram. In *2017 Progress In Electromagnetics Research Symposium - Spring (PIERS)*, 426–30. St Petersburg, Russia: IEEE. https://doi.org/10.1109/PIERS.2017.8261777.

Kutuzov, V. M., M. A. Ovchinnikov, and E. A. Vinogradov. (2021). Accuracy Characteristics of the Parametric Burg Method for Spatial Signal Processing in a Nonuniform Array Antenna. *Journal of the Russian Universities. Radioelectronics* 24, fasc. 3 : 60–71. https://doi.org/10.32603/1993-8985-2021-24-3-60-71.

Li, Xin, Hongbo Wang, Zhe Chen, Zhiping Jiang, and Jun Luo. (2024). UWB-Fi: Pushing Wi-Fi towards Ultra-Wideband for Fine-Granularity Sensing. In *Proceedings of the 22nd Annual International Conference on Mobile Systems, Applications and Services*, 42–55. Minato-ku, Tokyo Japan: ACM. https://doi.org/10.1145/3643832.3661889.

Liu, Wanchun, Xin Zang, Yonghui Li, and Branka Vucetic. (2020). Over-the-Air Computation Systems: Optimization, Analysis and Scaling Laws. *IEEE Transactions on Wireless Communications* 19, fasc. 8 : 5488–5502. https://doi.org/10.1109/TWC.2020.2993703.

Luca, M.B., S. Azou, G. Burel, and A. Serbanescu. (2005). A Complete Receiver Solution for a Chaotic Direct Sequence Spread Spectrum Communication System. In *2005 IEEE International Symposium on Circuits and Systems*, 3813–16. Kobe, Japan: IEEE. https://doi.org/10.1109/ISCAS.2005.1465461.

Nazer, B., and M. Gastpar. (2007). Computation Over Multiple-Access Channels. *IEEE Transactions on Information Theory* 53, fasc. 10 : 3498–3516. https://doi.org/10.1109/TIT.2007.904785.

Pavlikov, Vladimir V., Valeriy K. Volosyuk, Simeon S. Zhyla, and Nguyen Van Huu. (2018). Active Aperture Synthesis Radar for High Spatial Resolution Imaging. In *2018 9th International Conference on Ultrawideband and Ultrashort Impulse Signals (UWBUSIS)*, 252–55. Odessa: IEEE. https://doi.org/10.1109/UWBUSIS.2018.8520021.

Pavlikov, V. V., V. K. Volosyuk, and S. S. Zhyla. (2018). Ultra-wideband Passive radars Fundamental Theory and Applications. In *2018 IEEE 17th International Conference on Mathematical Methods in Electromagnetic Theory (MMET)*, 1–6. Kiev: IEEE. https://doi.org/10.1109/MMET.2018.8460251.

Pogorelyuk, Leonid, Laurent Pueyo, Jared R. Males, Kerri Cahoy, and N. Jeremy Kasdin. (2021). Information-theoretical Limits of Recursive Estimation and Closed-loop Control in High-contrast Imaging. *The Astrophysical Journal Supplement Series* 256, fasc. 2 : 39. https://doi.org/10.3847/1538-4365/ac126d.

Ramos-Perez, Isaac, Adriano Camps, Xavi Bosch-Lluis, Nereida Rodriguez-Alvarez, Enric Valencia-Domènech, Hyuk Park, Giuseppe Forte, and Merce Vall-llosera. (2012). PAU-SA: A Synthetic Aperture Interferometric Radiometer Test Bed for Potential Improvements in Future Missions. *Sensors* 12, fasc. 6 : 7738–77. https://doi.org/10.3390/s120607738.

Rojhani, Neda, Maria Sabrina Greco, e Fulvio Gini. CRLBs for Location and Velocity Estimation for MIMO Radars in CES-Distributed Clutter. *Frontiers in Signal Processing* 2 (25 marzo 2022): 822285. https://doi.org/10.3389/frsip.2022.822285.

Romero, Daniel, Seung-Jun Kim, Georgios B. Giannakis, and Roberto Lopez-Valcarce. (2017). Learning Power Spectrum Maps From Quantized Power Measurements. *IEEE Transactions on Signal Processing* 65, fasc. 10 : 2547–60. https://doi.org/10.1109/TSP.2017.2666775.

Sadiku, M.N.O., and C.M. Akujuobi. (2004). Software-Defined Radio: A Brief Overview. *IEEE Potentials* 23, fasc. 4: 14–15. https://doi.org/10.1109/MP.2004.1343223.

Saho, Kenshi, and Masao Masugi. (2015). Automatic Parameter Setting Method for an Accurate Kalman Filter Tracker Using an Analytical Steady-State Performance Index. *IEEE Access* 3 : 1919–30. https://doi.org/10.1109/ACCESS.2015.2486766.

Smiti, Abir, and Zied Elouedi. (2012). DBSCAN-GM: An improved clustering method based on Gaussian Means and DBSCAN techniques. In *2012 IEEE 16th International Conference on Intelligent Engineering Systems (INES)*, 573–78. Lisbon, Portugal: IEEE. https://doi.org/10.1109/INES.2012.6249802.

So, H. C. (2018). Source Localization: Algorithms and Analysis. In *Handbook of Position Location*, a cura di Seyed A. (Reza) Zekavat e R. Michael Buehrer, 1ª ed., 59–106. Wiley. https://doi.org/10.1002/9781119434610.ch3.

Tse, David, and Pramod Viswanath. (2005). *Fundamentals of Wireless Communication*. 1ª ed. Cambridge University Press. https://doi.org/10.1017/CBO9780511807213.

Unbehauen, Rolf, and Andrzej Cichocki. (1989). CMOS Analog-to-Digital and Digital-to-Analog Conversion Systems. In *MOS Switched-Capacitor and Continuous-Time Integrated Circuits and Systems*, di Rolf Unbehauen e Andrzej Cichocki, 555–627. Berlin, Heidelberg: Springer Berlin Heidelberg. https://doi.org/10.1007/978-3-642-83677-0_7.

Van Der Merwe, R., and E.A. Wan. (2001). The square-root unscented Kalman filter for state and parameter-estimation». In *2001 IEEE International Conference on Acoustics, Speech, and Signal Processing. Proceedings (Cat. No.01CH37221)*, 6:3461–64. Salt Lake City, UT, USA: IEEE. https://doi.org/10.1109/ICASSP.2001.940586.

Volosyuk, V. K., V. V. Pavlikov, and S. S. Zhyla. (2018). Phenomenological Description of the Electromagnetic Field and Coherent Images in Radio Engineering and Optical Systems. In *2018 IEEE 17th International Conference on Mathematical Methods in Electromagnetic Theory (MMET)*, 302–5. Kiev: IEEE. https://doi.org/10.1109/MMET.2018.8460321.

Wan, E.A., and R. Van Der Merwe. (2000). The unscented Kalman filter for nonlinear estimation. In *Proceedings of the IEEE 2000 Adaptive Systems for Signal Processing, Communications, and Control Symposium (Cat. No.00EX373)*, 153–58. Lake Louise, Alta., Canada: IEEE. https://doi.org/10.1109/ASSPCC.2000.882463.

Wanchun Tang, Songmao Yang, Xiaoke Wang, Cheng Wang, and Y. L. Chow. (2012). A novel UWB bandpass filter using highpass and lowpass filters. In *2012 4th International High Speed Intelligent Communication Forum*, 1–2. Nanjing, Jiangsu: IEEE. https://doi.org/10.1109/HSIC.2012.6212999.

White, Joseph F. (2003). *High Frequency Techniques: An Introduction to RF and Microwave Engineering*. 1ª ed. Wiley. https://doi.org/10.1002/0471474827.

Xiong, Kai, and Chunling Wei. (2018). Adaptive Iterated Extended KALMAN Filter for Relative Spacecraft Attitude and Position Estimation. *Asian Journal of Control* 20, fasc. 4 : 1595–1610. https://doi.org/10.1002/asjc.1689.

Xiong, Xinli, Kuan Wang, Jianbin Chen, Tao Li, Haoyun Deng, and Fan Ren. (2021). Parameter Adjustment Method of Kalman Filter Based on Quadratic Curve Fitting. In *2021 33rd Chinese Control and Decision Conference (CCDC)*, 780–83. Kunming, China: IEEE. https://doi.org/10.1109/CCDC52312.2021.9602678.

Zhang, Xue, Cihan Tepedelenlioglu, Mahesh Banavar, and Andreas Spanias. (2013). CRLB for the localization error in the presence of fading. In *2013 IEEE International Conference on Acoustics, Speech and Signal Processing*, 5150–54. Vancouver, BC, Canada: IEEE. https://doi.org/10.1109/ICASSP.2013.6638644.

Zhang, Z.G., W.Y. Lau, and S.C. Chan. (2006). A New Kalman Filter-based Power Spectral Density Estimation for Nonstationary Pressure Signals. In *2006 IEEE International Symposium on Circuits and Systems*, 1619–22. Island of Kos, Greece: IEEE. https://doi.org/10.1109/ISCAS.2006.1692911.